JOURNAL OF GEOPHYSICAL RESEARCH, VOL. 114, D12301, doi:10.1029/2008JD011237, 2009

Light-induced ozone depletion by humic acid films and submicron aerosol particles

Barbara D'Anna,[1] Adla Jammoul,[1] Christian George,[1] Konrad Stemmler,[2] Simon Fahrni,[2] Markus Ammann,[2] and Armin Wisthaler[3]

Received 3 October 2008; revised 6 February 2009; accepted 25 March 2009; published 17 June 2009.

[1] The interactions of ozone with submicron particles and films consisting of humic acids of various origins were investigated under near-ultraviolet and visible irradiation using aerosol and coated wall flow-tube systems. Ozone loss to these surfaces was strongly activated in the presence of irradiation. Under simulated atmospheric conditions with respect to irradiance, relative humidity, and O_3 mixing ratios, the reactive uptake coefficients of the coatings ranged from $\gamma \sim 10^{-6}$ (in the dark) to $\gamma \sim 10^{-4}$ (under near-UV and visible irradiation) and were inversely dependent on the ozone mixing ratio in the 20- to 270-ppbv range. For the aerosol experiment the uptakes were an order of magnitude smaller. Light and ozone exposure promoted emissions of volatile organic compounds including small aldehydes (formaldehyde, acetaldehyde, hexanal, octanal, nonanal), methanol, and acetone. These results together suggest the existence of photoinduced ozone removal at the surface of various humic substances, which may be a potentially important ozone sink in the continental boundary layer and can represent a possible pathway for processing the organic aerosol.

Citation: D'Anna, B., A. Jammoul, C. George, K. Stemmler, S. Fahrni, M. Ammann, and A. Wisthaler (2009), Light-induced ozone depletion by humic acid films and submicron aerosol particles, *J. Geophys. Res.*, *114*, D12301, doi:10.1029/2008JD011237.

1. Introduction

[2] Ozone is a key player in gas-phase atmospheric chemistry; it is a photolytic precursor of the OH radical, a selective oxidant and in addition, it is an important greenhouse gas. Its increase in the troposphere is estimated to provide the third largest contribution in direct radiative forcing since the pre-industrial era.

[3] Ozone is removed by several processes among those photochemical destruction, chemical removal and dry deposition are the most relevant [*Hauglustaine et al.*, 1998; *Wesely and Hicks*, 2000]. Ozone chemical loss occurs through reaction with unsaturated organic compounds (addition to double bonds), with one-electron donors such as phenolate ion [*Mvula and von Sonntag*, 2003] and with certain radicals (HO_2, NO, Cl, Br). The aqueous solution chemistry of ozone toward organic species (dicarboxylic and monocarboxylic acids, phenols, alcohols, humic matter) has been extensively studied in the past [*Hoigné and Bader*, 1983; *Staehelin and Hoigne*, 1983; *Staehelin and Hoigne*, 1985]. Ozonation of natural organic matter (NOM) in solution causes a decrease of the UV absorbance and of the average molecular weight, while polarity and acidity increase [*Amy et al.*, 1988; *Chiang et al.*, 2006; *Cho et al.*, 2003; *Garcia-Araya et al.*, 1995; *Gorski et al.*, 1996; *Guittonneau et al.*, 1996; *Kruithof et al.*, 1989; *Mallevialle et al.*, 1978; *Nawrocki and Kalkowska*, 1999; *Staehelin and Hoigne*, 1983; *Swietlik et al.*, 2004; *Thomson et al.*, 2004; *von Gunten*, 2003; *Yu et al.*, 2002]. In solution, ozone decays in chain reactions, forming hydroxyl radical, which unselectively oxidizes organic compounds [*Hoigné and Bader*, 1983; *Staehelin and Hoigne*, 1983, 1985].

[4] The described reactions may be relevant for all environments containing organic matter and water such as lakes, rivers, soil and possibly atmospheric aerosols. In the past, they have therefore obtained considerable attention in the context of aquatic ecosystems. However, they have not been studied in detail in an atmospheric chemistry context. Little direct evidence exists on ozone depletion in the troposphere by direct interaction with clouds or aerosols [*Jacob*, 2000], except for certain arctic spring conditions, where ozone is significantly depleted owing to bromine radical chemistry in the gas phase, partially driven by supply of bromine from the aerosol phase [*Barrie et al.*, 1988; *Hausmann and Platt*, 1994]. Jacob et al. state the need of investigating the role of organic aerosols as a possible sink for ozone, as this type of aerosol has a sufficient source strength and potentially a high enough reactivity to provide a significant sink for ozone in the continental boundary layer [*Jacob*, 2000].

[5] The focus of this study is the reaction of ozone with humic acids (HA). These substances represent the most

[1]UMR5256, Institut de Recherches sur la Catalyse et l'Environnement de Lyon, Université Lyon 1, CNRS, Villeurbanne, France.
[2]Laboratory of Radio and Environmental Chemistry, Paul Scherrer Institute, Villigen, Switzerland.
[3]Institut für Ionenphysik und Angewandte Physik, Universität Innsbruck, Innsbruck, Austria.

0148-0227/09/2008JD011237$09.00

abundant group of organic species on the Earth's surface, originating from degradation of biological material [*Batjes*, 1996; *Janzen*, 2004; *Swift*, 2001]. As they are ubiquitously found on ground surfaces, a fraction can likely be present on airborne surfaces (owing to soil abrasion). Part of the organic fraction of aerosol particles resembles humic substances and is therefore called the Humic-Like substances (HULIS) [*Dinar et al.*, 2007, 2008; *Graber and Rudich*, 2006]. The analysis of its water soluble fraction showed the presence of aromatic, alcoholic, carboxylic and polycarboxylic functionalities [*Cappiello et al.*, 2003; *Decesari et al.*, 2006; *Salma and Lang*, 2008], molecular weight up to 700 Dalton with concentrations of 0.2–5.4 $\mu g/m^3$, corresponding to 8–45% of the total organic carbon. HULIS only partly resemble humic material, because they present much lower aromaticity, lower molecular weight and better droplet activation ability. Possible sources of tropospheric high molecular weight organic material can include photooxidation of gaseous precursors [*Baltensperger et al.*, 2005; *Dommen et al.*, 2006; *Mochida et al.*, 2007; *Reinhardt et al.*, 2007] and combustion processes, like biomass burning or fossil fuel combustion [*Decesari et al.*, 2002; *Gonzalez-Perez et al.*, 2004; *Hoffer et al.*, 2004; *Holmes and Petrucci*, 2006; *Kirchstetter et al.*, 2004; *Mayol-Bracero et al.*, 2002].

[6] In the present paper, we investigated the kinetics of ozone uptake to aerosol and stationary thin coatings of HA. The work has been motivated by the evidence that the heterogeneous reactive loss of gas-phase NO_2 and ozone at surfaces containing photoactive compounds may be significantly enhanced under illumination [*George et al.*, 2005; *Jammoul et al.*, 2008; *Stemmler et al.*, 2006, 2007]. In the case of NO_2, a good portion of the enhancement is due to heterogeneous reduction of the gas-phase compound to HONO, following photoexcitation of the substrate [*George et al.*, 2005; *Stemmler et al.*, 2006, 2007]. The substrates which demonstrate this effect to the greatest extent are those which act as photosensitizing or photoreducing agents [*Stemmler et al.*, 2006, 2007].

[7] The photoreactivity of samples from Aldrich, Elliot soil, Pahokee peat and Leonardite, has been investigated as a function of the irradiance, humidity and ozone mixing ratio. All the coatings experiments showed a comparable and important ozone uptake under simulated atmospheric conditions. Even though the reactivity of ozone with airborne humic substances does not realistically represent the reactivity of HULIS, the amount of ozone reacted may be significant for aerosol aging.

2. Experimental Section

[8] Three different experimental setups were used to explore the changes in HA reactivity toward ozone under illumination. All the systems were operated at room temperature and atmospheric pressure. The two coated flow-tube systems were quite similar (sections 2.1 and 2.2); the main differences were the flow rates (i.e., the residence time of the gas trace inside the tube), the intensity of the irradiation, the surface of the Pyrex support (one flat the other sandblasted) and the humidity. The third experiment (section 2.3) was carried out on submicron particles in an aerosol flow-tube system.

2.1. Flow-Tube Experiment 1 (IRCELYON)

[9] The kinetics data were determined using an atmospheric pressure-coated wall flow tube. The system consisted of Pyrex tube (0.55 cm inner radius, 20 cm length, inner surface = 69 cm^2, S/V = 3.64 cm^{-1}). The organic film is deposited inside the Pyrex tube and inserted into a photoreactor cell maintained at constant temperature, 290–293 K, using a circulating water bath through the outer jacket (Huber CC 405).

[10] The organic coating was prepared by depositing and drying of 0.5 mL of a 1 mg/mL HA solution in the inner section of a Pyrex tube. The carrier gas flows (synthetic air, O_3 and N_2 for dilution) were controlled by mass flow controllers and were varied from 170 to 180 mL/min ensuring a laminar flow regime (Reynolds's number < 15) and a residence time between 1.8 and 7 s (depending on the injector position). The experiments were performed at very low relative humidity ($\leq$5%). Ozone was produced by a mercury lamp irradiating an O_2 flow in a quartz cuvette. The ozone concentration was detected at the exit of the flow tube using a photometric ozone analyzer THERMO 49C (optical detection at 252 nm).

[11] The flow tube was surrounded by six fluorescent lamps: either visible Phillips TLD15W/54 in the range of 390–690 nm or UV-Black Light Blue OSRAM Sylvania TLD15W/08 ranging from 340 to 400 nm. The spectral irradiance $E(\lambda)$ reaching the inner surface of the reactor was quantified previously [see *Jammoul et al.*, 2008]. The spectral irradiance for the different sets of lamps is shown in Figure 1 together with a typical solar spectral irradiance at the Earth surface (standard spectral irradiance for solar zenith of 48°) [*Gueymard et al.*, 2002]. The absorption spectrum of Aldrich Humic Acid in aqueous solution is also shown as a medium dashed line (right scale) in Figure 1.

[12] In a subset of experiments, a Proton-Transfer-Reaction Mass Spectrometry (PTR-MS) instrument was connected immediately downstream of the flow reactor to detect volatile organic compounds (VOCs) emitted from the ozonized and/or irradiated HA films. PTR-MS is a well-established chemical ionization technique for the detection of VOCs [*de Gouw and Warneke*, 2007; *Lindinger et al.*, 1998]. The instrument was operated in the routine 120-Td mode of operation (1 Td = 10^{-17} cm^2 V $molecule^{-1}$). Mass scans were taken in the range of m/z 20 to 200. Quantification was based on calibration measurements using certified standards (prepared by Apel-Riemer Environmental Inc., Broomfield, Colorado).

2.2. Flow-Tube Experiment 2 (PSI)

[13] The PSI setup system consisted of a 50 cm × 0.8 cm Duran glass coated wall flow tube, installed in an air-cooled lamp housing holding seven fluorescence lamps surrounding the flow tube. The whole inner surface of the tubular glass flow tube (surface = 125 cm^2, surface to volume ratio = 5 cm^{-1}) was coated with a thin layer of humic acids (HA). The HA coatings were produced by gently drying 10.5-mL aliquots of aqueous solutions (1 mg/mL) of the HA dispersed on the tube walls in a nitrogen stream at room temperature. In general, a quantity of 1 mg of HA (8 μg cm^{-2}) was used as coating. The reactor surface was sandblasted to prevent

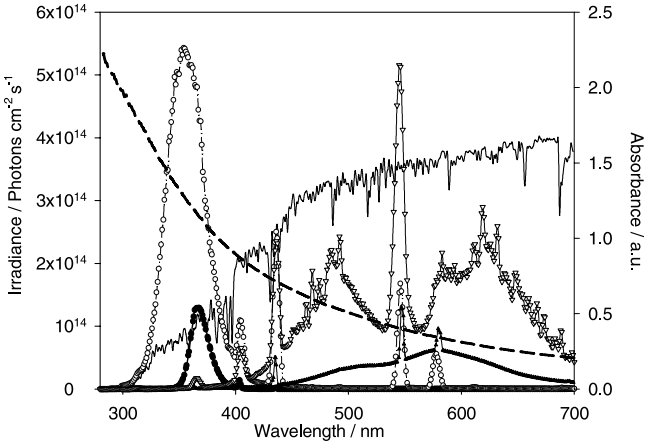

Figure 1. Spectral irradiance of the different light sources used in the present study. Empty circles: near-UV lamps used in the flow-tube setup 2 (PSI), the total irradiance in the 300- to 420-nm range is 2.4×10^{16} photons cm^{-2} s^{-1}. Solid circles are near-UV lamps used in flow-tube setup 1 (IRCELYON); total irradiance in the 340- to 420-nm range is 2.7×10^{15} photons cm^{-2} s^{-1}. Open triangle down is visible lamp used in flow-tube setup 2 (PSI); total irradiance in the 400–750 nm range is 4.4×10^{16} photons cm^{-2} s^{-1}. Solid diamonds are visible lamp used in flow-tube setup 1 (IRCELYON); total irradiance in the 400- to 750-nm range is 1.0×10^{16} photons cm^{-2} s^{-1}. Solid line is a typical solar spectral irradiance for solar zenith of 48° clear skies (1.9×10^{16} photons cm^{-2} s^{-1} between 300 and 420 nm and 1.0×10^{17} photons cm^{-2} s^{-1} between 400 and 700 nm) derived from the standard spectrum of the American Society for Testing and Materials (ASTM), which is tilted 37° tilted toward the Sun. The absorption spectrum of HA Aldrich in solution (pH 6, 100 μg mL^{-1}) is shown as a dashed line (right scale).

droplet formation during the coating procedure and therefore to reach a relatively homogeneous distribution of the HA.

[14] The carrier gas flows (N_2/O_2 = 4/1) were controlled by mass flow controllers, and the flow rate was normally 1.05 L min^{-1} at ambient pressure leading to gas residence times of 1.4 s under laminar flow conditions (Reynolds number 190). Usually, the experiments were performed at about 20–30% relative humidity. The gas temperature in the reactor was 303–305 K during irradiation. Ozone was produced by a UV-C lamp irradiating an O_2 flow in a quartz cuvette. The ozone concentration was monitored with a photometric ozone analyzer (model ML 9810, Monitor Labs Inc.) downstream of the reactor.

[15] The lamps used were either Osram Luminux Deluxe 954 daylight fluorescence lamps (400–750 nm, 15 W) or Phillips Cleo Compact tanning lamps (300–420 nm, 20 W). The spectral irradiance $E(\lambda)$ reaching the reactor cell surface was measured with a LI-COR 1800 hemispherical, cosine corrected spectroradiometer and it is shown in Figure 1. The isotropy of the irradiance in the reactor was confirmed with an International Light IL1700 photometer with SED 033 Silicon detector by measuring the total irradiance at the flow cell in different directions.

2.3. Aerosol Flow-Tube Experiment

[16] The experiments were performed in a 175 cm × 8 cm (i.d.) Duran glass aerosol flow tube at atmospheric pressure. The flow tube was equipped with two movable 20-cm Teflon plugs that allow adjusting the gas aerosol contact time between 5 and 25 min. The particles were produced by nebulizing a solution containing 20 g L^{-1} Aldrich HA sodium salt acidified to pH 4.5 with H_2SO_4 into a flow of N_2. The HA aerosol was initially dried in a 1.2-m-long Silica Gel diffusion drier, then sent through a bipolar ion source (^{85}Kr source) to establish an equilibrium charge distribution. Then all charged particles were removed in an electrostatic precipitator (with a voltage of 3 kV). Working with electrically neutral particles drastically reduces particle losses to the wall since they may now be removed via diffusion only. The neutral particles are then rehumidified to the desired relative humidity and mixed with a prehumidified stream of air and O_3.

[17] A small portion of the flow was diluted by a factor of 3 with humidified N_2 and directed to a Scanning Mobility Particle Sizer (SMPS) consisting of a Differential Mobility Analyzer (TSI Model 3071) and a Condensation Particle Counter (TSI, Model 3022). The total aerosol surface ranged from 0.2 to 0.31 m^2 m^{-3}, with particles having roughly a lognormal size distribution with a mode at 100 nm. The gas-aerosol mixture then entered the reactor at a flow rate of 650 mL/min.

[18] At the exit of the reactor the flow was separated and sent to the ozone detector and to an electrometer to monitor the aerosol concentration. For the latter, the aerosol was recharged using a ^{85}Kr source and deposited in the annular space of a flow-through capacitor loaded by a 600-V battery, the resulting current was monitored by the electrometer. This signal provides an online proxy of aerosol surface area with high time resolution that can be calibrated with the SMPS system. The aerosol was physically separated from the ozone in an annular coflow device; two flows, one from the reactor (250 mL min^{-1}) and a sheath flow of particle free air (350 mL min^{-1}), were used to allow ozone diffusing from the former into the latter. The particle free gas was then sent to the ozone analyzer and the gas concentration was corrected for the dilution ratio in the separator.

[19] The reactor was installed in an air cooled lamp housing holding seven fluorescence lamps (150 cm × 2.6 cm o.d.) surrounding the reactor tube. Philips Cleo Effect UV-A tanning lamps (70 W 300–420 nm) were employed as the light source. Their spectral distribution is very similar to that of the Phillips Cleo Compact tanning lamps shown in Figure 1. The spectral actinic flux in the reactor was measured by a calibrated spectroradiometer [*Hofzumahaus et al.*, 1999] with an optical receiver scaled down for the measurements in the flow tube and corrected for the imperfect angular response. The total irradiance in the 300–420 nm range was 5.1×10^{16} photons cm^{-2} s^{-1}.

2.4. Chemicals

[20] All chemicals were used without any further purification: HA sodium salt (Aldrich, 98%), sulfuric acid (Sigma-Aldrich 95–98%), sodium hydroxide solution 32% (Riedel-de Haën). The pH was adjusted using NaOH

or H_2SO_4 solutions (10^{-3} M) and measured using a pH meter (PHM210 MeterLab Radiometer Analytical).

[21] Three humic acid (HA) samples Elliott Soil HA Standard, Leonardite HA Standard, and Pahokee Peat HA Reference were purchased from the International Humic Substances Society (IHSS). Elliott Soil HA Standard is extracted from a fertile prairie soil in the U.S. state of Illinois. The Elliott soil consists of very deep, somewhat poorly drained soils on moraines and till plains. Leonardite HA Standard is produced by the natural oxidation of exposed lignite, a low-grade coal. The sample was obtained from a Gascoyne Mine in North Dakota. The Pahokee Peat HA is a typical agricultural peat soil of the Florida Everglades. The IHSS sample was obtained from the University of Florida Belle Glade Research Station. The Pahokee series consists of very poorly drained soils that are 36 to 51 inches thick over limestone. The fourth HA was purchased from Aldrich, for which no origin is specified.

[22] C, H, O, N, S, and P are the elemental composition in % (w/w) of a dry, ash-free sample provided by the suppliers. Chemical analysis shows high C contents in the three IHSS samples with percentages ranging from 56 to 64%, while the Aldrich sample contained 39% of C; the H, O, N and S content was between 3.7 and 4.6%, 31–37%, 0.6–4.1% and 0.4–0.9%, respectively. Inorganic trace element analysis was available only for the Aldrich Humic Acid, for which the major constituents are Na 8.7%, Ca 1.4%, Si 0,8%, Fe 0.6%, Al 0.4% and Mg 0.3%. Prior to use, the Pyrex tubes were cleaned using a solution of sodium hydroxide (1M), distilled water, then a sulfuric acid solution (0.5 M) and again water.

3. Kinetics

[23] The loss of gas-phase ozone in the flow tube was measured as a function of injector position, which was related to different gas/solid contact times using the known total flow velocity. A single exponential fit of the measured ozone concentration at one (PSI) and several (IRCELYON) exposure times were used to derive an apparent pseudo-first-order observed coefficient (k) for the ozone decay:

$$(1 - \Delta n/n) = \exp(-kt), \tag{1}$$

where n is the ozone concentration at the flow-tube entrance, Δn is the ozone consumed, t is the residence time. Each kinetics (IRCELYON setup) was measured on a freshly prepared coating (a new film was prepared for each experimental data point) and data from several exposure times were analyzed using a weighted least squares procedure including uncertainties associated with the ozone concentration and the residence time, allowing a zero-point offset [*York*, 1966]. Since gas trace uptake depends on several steps as adsorption/desorption and chemical reaction at the surface sites, the total quoted uncertainties should take into account a combination of estimated errors for the different variables and can be expressed as

$$\left[\left(\frac{\Delta F_{O3}}{F_{O3}}\right)^2+\left(\frac{\Delta F_T}{F_T}\right)^2+\left(\frac{\Delta T}{T}\right)^2+\left(\frac{\Delta R}{R}\right)^2+\left(\frac{\Delta k}{k}\right)^2\right]^{1/2},$$

where F_{O3} and F_T are the ozone and total flow rates (STP), T is the temperature in Kelvin, R is the inner tube radius, k is the pseudo-first-order coefficient. The total uncertainty is approximately 15–30% for the IRCELYON data. For the PSI setup, the errors were estimated on the basis of the standard deviation of the results of the n repetitions of the experiment.

[24] The derived pseudo-first-order coefficient is related to the uptake coefficient (γ) through equation (2),

$$k = \gamma\langle c\rangle[S/V]/4, \tag{2}$$

where $\langle c\rangle$ is the ozone mean thermal velocity $(8RT/\pi M)^{0.5}$ and $[S/V]$ is the surface/volume concentration measured during the experiment.

[25] Equations (1) and (2) were used for the aerosol experiments and those coated wall flow-tube experiments, where the overall ozone loss was smaller than about 30%. These equations are not applicable if gas-phase diffusion limitations exist, i.e., when radial gas concentration profiles build up, and this could occur if the loss at the surface is faster than diffusion could replenish the near-surface region. In the case of more substantial ozone loss, the uptake coefficient was calculated by using the Cooney-Kim-Davis (CKD) method [*Cooney et al.*, 1974], which takes into account axial and lateral diffusion combined with a first-order loss at the inner surface of a cylindrical tube under laminar flow conditions. We used an implementation of this method described previously [*Ammann et al.*, 2005]. Using this procedure, the measured loss of ozone was fitted using the uptake coefficient as the only free parameter. The diffusion coefficient D was calculated using the formula proposed by *Fuller et al.* [1969] and molecular diffusion volumes of 17 $cm^3\ mol^{-1}$ for O_3 and 18.5 $cm^3\ mol^{-1}$ for N_2.

[26] The reactive uptakes have been evaluated at two ozone exposure times: after 5–10 min giving the uptake coefficient (γ) and sometimes after 40–50 min of exposure, when the gas concentration profile of the dark experiment reached a plateau, in this case the kinetic value was defined as steady state uptake coefficient (γ_{ss}).

[27] Ozone loss through direct photolysis has been evaluated for the PSI experimental setup, which employs near-UV irradiation starting at 300 nm. Direct photolysis and possible formation of $O(^1D)$ accounts for less than 2% of the total ozone loss in the aerosol flow tube, which is characterized by a maximum residence time of 25 min. Direct photolysis is therefore negligible both in the aerosol flow tube and in the coated flow tube (PSI), where the residence time is less than 2 s. In the IRCELYON setup the near-UV irradiation starts at 340 nm, and thus direct ozone photolysis is negligible.

4. Results and Discussion

[28] The most significant results may be summarized as follows: under illumination, the reactive loss of ozone on HA coatings and aerosol is significantly enhanced. During processing of HA coatings emission of light VOCs is observed. Additional detailed studies demonstrate that the ozone loss is highly dependent on the experimental conditions like irradiation type and intensity, ozone mixing ratio, humidity, and pH of the starting solution.

4.1. Ozone Dark Versus Irradiation

[29] Figure 2 shows typical raw ozone profiles of HA coatings and aerosol under dark and light conditions. The plots presented here emphasize the existence of a light-induced process, which causes significant ozone destruction at the surface of the four HA and may persist for many hours. In Figures 2a–2c the gray arrow represent the periods of exposure to ozone under dark reaction, while the white arrows represent the exposure under irradiation. Tests on the bare glass surface showed neither dark nor photochemical destruction of ozone. Figure 2c presents the ozone profile on Pahokee Peat HA using clear sky sunlight (8 September 2005, 1700 local time at PSI, Villigen, Switzerland; Zenith angle 71°). Under these conditions an irradiance of 1.1×10^{17} photons cm^{-2} s^{-1} in the 300- to 700-nm wavelength range is modeled using the tropospheric Ultraviolet and Visible Radiation Model (TUV) (National Center for Atmospheric Research, Tropospheric Ultraviolet and Visible (TUV) radiation model, 2006, http://cprm.acd.ucar.edu/Models/TUV/) for an ozone column of 300 DU, a surface albedo of 0 and a standard aerosol of the model. This value is comparable to the irradiance determined experimentally in the reactor for the visible irradiation. All the dark experiments are characterized by a large initial ozone uptake that rapidly decreases to a nonzero value after exposure times of 15–30 min (Figures 2a–2d). In contrast, when the coating is exposed to near-UV and/or visible irradiation ozone loss is larger and lasts longer. The environmental relevance of the ozone removal observed here is linked to its kinetics and to the overall capacity of a given amount of HA to remove a trace gas. To assess the latter, the time dependence of the process was investigated by exposing a HA film to 25 ppbv of ozone for approximately 6 h (Figure 2d). The results confirm what previously observed, i.e., a rapid decrease of the reactivity under dark conditions (solid line), while under near-UV irradiation (open circles) the reactivity is more important and lasts for approximately 6 h. At the end of the experiment under dark conditions the coating was briefly exposed to near-UV irradiation and high photoreactivity of the HA film (Figure 2d) was observed. Figure 2e shows the ozone profile during the aerosol flow-tube experiment under near-UV irradiation. The plot clearly correlates the ozone decrease (right axis) with the presence of the HA aerosol, monitored by the current detected by the electrometer. The relatively slow recovery of the ozone signal to its initial value can be explained by gas reaction with some aerosol deposit in the system. The uptake coefficient was calculated from the measured difference of ozone concentration in presence and absence of aerosol in the reactor and using equations (1) and (2).

4.2. Quantitative Analysis

[30] A summary for the geometric uptake coefficients of O_3 toward the HA coatings is compiled in Table 1. The different HA show a photoenhanced ozone loss under simulated solar irradiation despite the different origins and characteristics of the substrates. Under dark conditions the uptake coefficients range from (2.9 ± 1.6) to $(3.8 \pm 0.3) \times 10^{-6}$. Upon irradiation with visible light at an irradiance of 4.4×10^{16} photons cm^{-2} s^{-1} in the spectral range 400–750 nm (37% of the solar irradiance, standard spectra given in Figure 1) the uptake increased by approximately a factor of 3–8 reaching uptake coefficients of (1.0 ± 0.6) and $(3.0 \pm 0.9) \times 10^{-5}$. Under an intense UV-A irradiation (2.4×10^{16} photons cm^{-2} s^{-1}, which corresponds to 126% of the solar irradiance given in Figure 1) the observed uptake coefficients increased by a factor of 9–21 compared to the dark experiment, reaching uptake coefficients of (2.7 ± 0.6) and $(7.8 \pm 0.9) \times 10^{-5}$. Note that coefficients of this magnitude are close to the diffusion limit of the coated wall flow-tube setup and are therefore associated with a significant uncertainty.

4.3. Effect of Irradiance

[31] In Figure 3, the linear dependence of the reaction on the photon flux is shown. Figure 3 presents the ozone uptake on HA Aldrich coating and submicron aerosol particles under near-UV irradiation and on Pahokee Peat films under visible irradiation. Although the reactivity is dependent on many parameters, among others the ozone mixing ratio (see below), Figure 3 can be carefully used to scale the measured uptake coefficients to more realistic atmospheric conditions, given the apparent linear dependence of the uptake coefficient on irradiance. This procedure is quite useful when the irradiance used in the experimental setup is quite different from that reaching the troposphere or the Earth surface. For the near-UV experiments at PSI (Table 1) the kinetic data represent an upper limit value, since in the reactor the irradiance was $\sim 2.4 \times 10^{16}$ photons cm^{-2} s^{-1}, while in the atmosphere in the same wavelength range (300–420 nm) the irradiance is approximately $\sim 1.9 \times 10^{16}$ photons cm^{-2} s^{-1} [*Gueymard et al.*, 2002]. Using the linear fit obtained for 30 ppbv of ozone (solid circles) the near-UV uptake coefficients on thin coatings can be scaled to $(6.1 \pm 0.7) \times 10^{-5}$. Under visible irradiation the calculated uptake coefficients represent a lower limit value since at the Earth surface the irradiance is $\sim 1.0 \times 10^{17}$ photons cm^{-2} s^{-1} in the 400- to 700-nm range [*Gueymard et al.*, 2002], while the visible lamps had an irradiance of $\sim 4.4 \times 10^{16}$ photons cm^{-2} s^{-1}. If the linearity found in Figure 3 is extrapolated to the solar spectral irradiance at the Earth surface under visible irradiation, the uptake coefficient derived at 30 ppbv of ozone becomes $(5.4 \pm 1.4) \times 10^{-5}$. These results strongly suggest that photoenhanced destruction of ozone on thin coatings of different humic substances is very important under environmental conditions and particularly under the visible irradiation present at the Earth surface.

4.4. Effect of Ozone Mixing Ratio

[32] The dependence of the observed ozone loss rate on its initial concentration, photon flux and HA type is illustrated in Figure 4. The experimental results include data from both setups: PSI (open symbols) and IRCELYON (solid symbols). Figure 4 shows an inverse dependence on the ozone mixing ratio that becomes more pronounced at higher photon flux. The latter has tentatively been explained by the larger reactivity of the film under higher photon flux irradiation.

[33] The inverse dependence on the gas reagent can suggest a Langmuir-Hinshelwood surface-mediated reaction, in which ozone is in rapid equilibrium between the gas and solid phase and the reaction takes place between adsorbed species. Similar gas reactant dependence has been

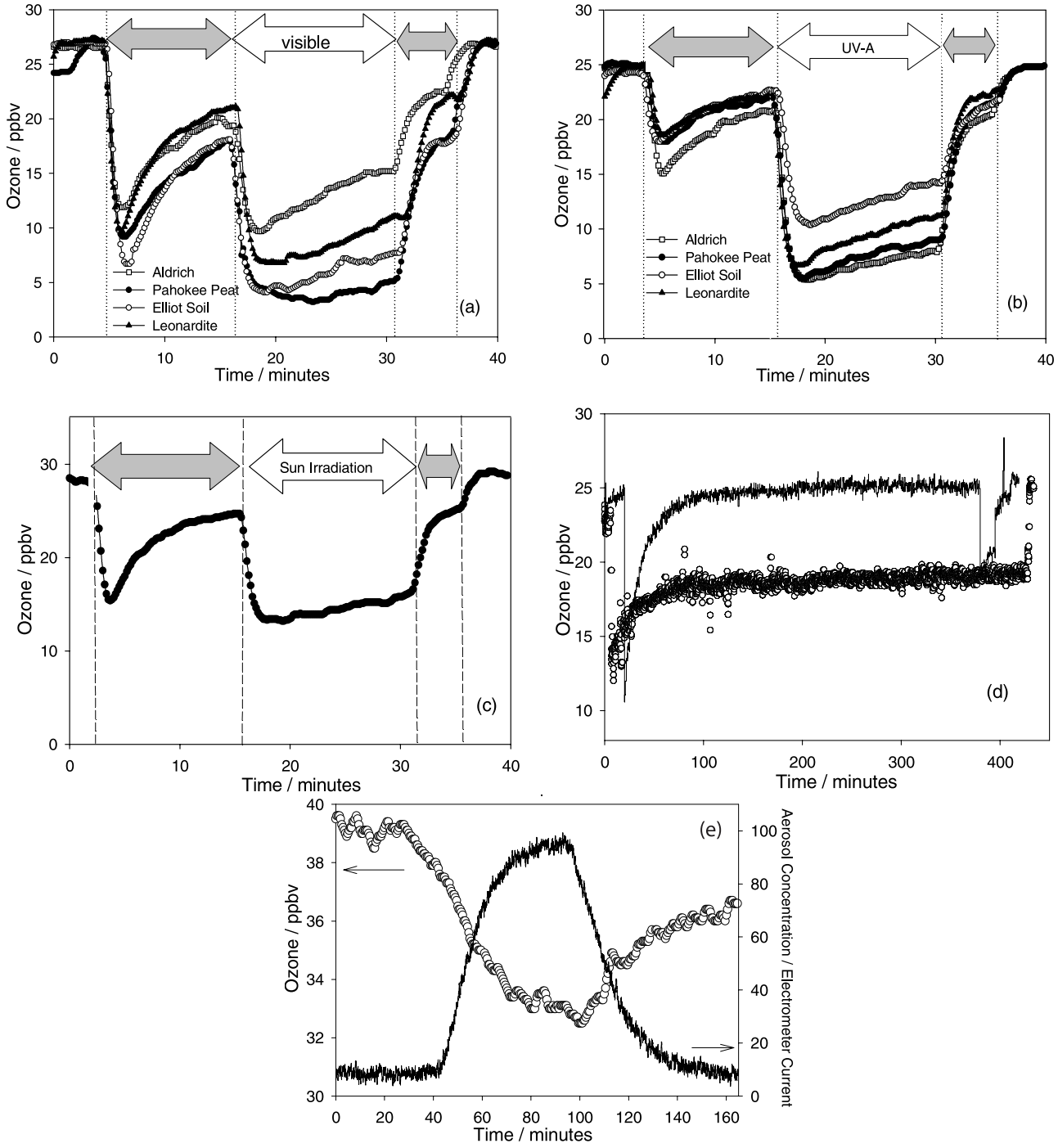

Figure 2. Raw ozone profile for HA coatings and aerosol experiments. (a and b) Comparison of the ozone loss on 8 μg cm^{-2} of HA Aldrich sodium salt (open square), Pahokee Peat (solid circle), Elliot Soil (open circle), and Leonardite (solid triangle) exposed to different type of irradiation (pH 4.5 and 25% RH). The gray arrows indicate periods where the humic acid was exposed to ozone in the dark, and the white arrows indicate the period of irradiation. Figure 2a is experiment with artificial visible irradiation (400–750 nm, irradiance 1.1 $\times$ 10^{17} photons cm^{-2} s^{-1}). Figure 2b is experiment with artificial near-UV irradiation (300–420 nm, irradiance of 2.4 $\times$ 10^{16} photons cm^{-2} s^{-1}). (c) Experiment on Pahokee Peat coating exposed to natural solar light (estimated solar flux of 1.1 $\times$ 10^{-17} photons cm^{-2} s^{-1}). (d) Ozone profile on HA Aldrich film (pH 6, 5% RH and 7 μg cm^{-2}) during approximately 6 h of exposure to ozone under dark condition (solid line) and near-UV irradiation (open circles, 340–420 nm, irradiance 2.7 $\times$ 10^{15} photons cm^{-2} s^{-1}). (e) Ozone profile (open circles) on HA Aldrich aerosol (solid line, pH 4.5, 25% RH) under near-UV irradiation (300–420 nm, irradiance 5.1 $\times$ 10^{16} photons cm^{-2} s^{-1}).

Table 1. Comparison of the Ozone Uptake Coefficients on Thin Coatings of Different HA in the Dark and Under Visible and Near-UV Irradiation[a]

	HA Aldrich	Elliott Soil HA Standard	Leonardite HA Standard	Pahokee Peat HA Reference
Uptake coefficient dark conditions	$3.6(\pm1.7) \times 10^{-6}$ $n = 9$	$2.9(\pm1.6) \times 10^{-6}$ $n = 10$	$3.8(\pm0.3) \times 10^{-6}$ $n = 3$	$3.6\ (\pm1.9) \times 10^{-6}$ $n = 15$
Uptake coefficient visible irradiation[b]	$1.0(\pm0.6) \times 10^{-5}$ $n = 4$	$2.0 \times (\pm0.7) \times 10^{-5}$ $n = 5$	$1.4(\pm0.4) \times 10^{-5}$ $n = 2$	$3.0(\pm0.9) \times 10^{-5}$ $n = 10$
Uptake coefficient UV-A irradiation[c]	$7.8(\pm0.8) \times 10^{-5}$ $n = 5$	$2.7 \times (\pm0.6) \times 10^{-5}$ $n = 5$	3.7×10^{-5} $n = 1$	$5.5(\pm1.4) \times 10^{-5}$ $n = 5$

[a]The values are reported for 25 ppbv of O_3 on 8 μg cm^{-2} of HA (PSI setup) at 25% RH. The humic acid starting solutions were acidified to pH 4.5 or pH 6 using either H_2SO_4 or H_3PO_4. The errors reported are the standard deviation of the results of the n repetitions of the experiment.
[b]Irradiance spectrum: see Figure 1 (4.4×10^{16} photons cm^{-2} s^{-1} in the 400- to 750-nm range).
[c]Irradiance spectrum: see Figure 1 (2.4×10^{16} photons cm^{-2} s^{-1} in the 300- to 420-nm range).

previously observed in many heterogeneous studies of organic surfaces including polycyclic aromatic hydrocarbons [*Mmereki and Donaldson*, 2003; *Mmereki et al.*, 2004; *Poeschl et al.*, 2001], oleic acid salts [*McNeill et al.*, 2007], chlorophyll [*Clifford et al.*, 2008] and humic acids [*Stemmler et al.*, 2007]. The basis for the explanation of the inverse dependence on O_3 concentration comes from the fact that at all O_3 concentrations, the reagent signal reached a quasi steady state that even after 12 h did not return to the original value. The time to reach this steady state was also not changing with ozone concentration. Therefore, the idea of a precursor mediated uptake process is a reasonable explanation. A precursor whose density on the surface (or in the bulk) is limited seems to be responsible for the observed O_3 dependence. However, other processes cannot be excluded. *Rapoport et al.* [1968] and more recently *Emeline et al.* [2005] showed that for heterogeneous photocatalytic reactions a similar dependence of the pseudo-first-order heterogeneous reaction rate on the gas-phase reagent concentration may be obtained in absence of a rate-limiting adsorptive step.

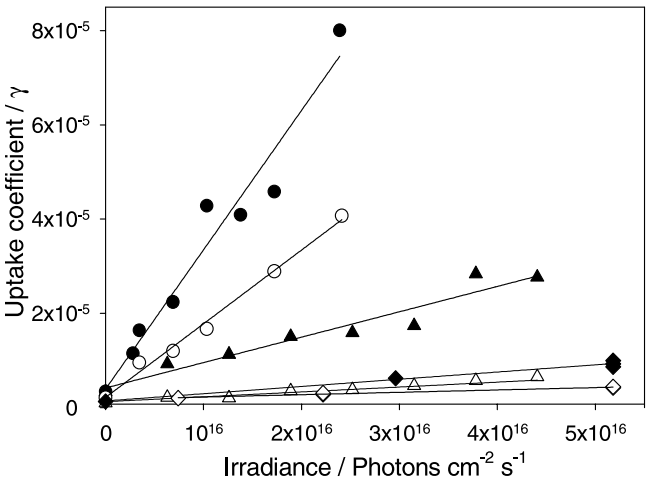

Figure 3. Ozone uptake coefficient as a function of irradiance (photons cm^{-2} s^{-1}) for near-UV and visible irradiation on thin coatings (8 μg cm^{-2}) and submicron aerosols. The circles correspond to the near-UV experiment on a HA Aldrich film (pH 4.5) at 30 ppbv (solid circles) and 79 ppbv (open circles) of ozone. The triangles represent the visible experiment on a Pahokee Peat film (pH6) at 25 ppbv (solid triangles) and 100 ppbv (open triangles). The diamonds represent the UV-A experiment (400–700 nm) on submicron aerosol particles of HA Aldrich (pH 4.5) at 50 ppbv (solid diamonds) and 65 ppbv (open diamonds) of ozone.

4.5. Effect of Humidity

[34] Water partial pressure is another important variable parameter in the natural environment and Figure 5 presents the ozone loss (first 10 min) on HA coatings when the relative humidity varied from 5 to 65%. Figure 5 clearly shows a completely different effect of humidity on the ozone removal under irradiation (open circles) as compared to dark conditions (solid symbols). The dark reaction is characterized by a weak linear positive dependence on the partial pressure of water, with uptake coefficients increasing from $(1.6 \pm 0.7) \times 10^{-6}$ at very low humidity ($\leq$7%) to $(4.0 \pm 0.5) \times 10^{-6}$ at 50%. The NO_2 shows the same humidity dependence in the dark with model compounds and HA [*Arens et al.*, 2002; *Stemmler et al.*, 2007]. NO_2 is less

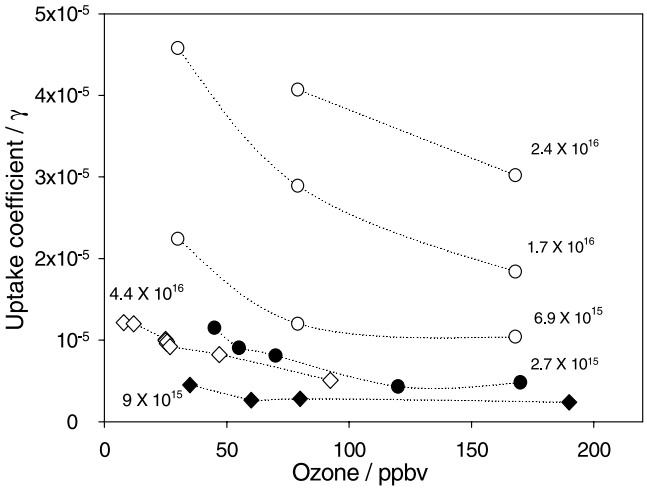

Figure 4. Dependence of the reactive uptake on ozone mixing ratio for HA thin coatings (8 μg cm^{-2}) using different irradiation type and intensity. The values on the graph correspond to the total irradiance (number of photons cm^{-2} s^{-1}) reaching the coating. Open circles are ozone uptake on HA Aldrich (pH 4.5, RH 25%) during near-UV irradiation ($300 < \lambda < 420$ nm, Figure 1 open circles). Solid circles are ozone uptake on HA Aldrich (pH 6, RH 7%) under near-UV irradiation ($340 < \lambda < 420$ nm, Figure 1 solid circles). Open diamonds are ozone uptake on HA Pahokee Peat (pH 6, RH 25%) under visible irradiation ($300 < \lambda < 700$ nm Figure 1 open triangles). Solid diamonds are ozone uptake on HA Aldrich (pH 6, RH 7%) under visible irradiation ($300 < \lambda < 700$ nm Figure 1 solid diamonds).

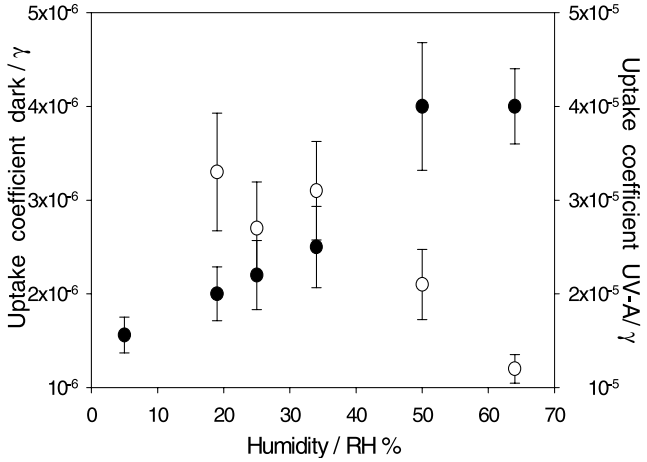

Figure 5. Dependence of the uptake coefficient γ of O_3 on the relative humidity during near-UV irradiation at 2.4×10^{16} photons $cm^{-2}s^{-1}$ in the range 300–420 nm (open circles) and under dark (solid circles) reaction. The organic coatings (8 μg cm^{-2}) consisted of Pahokee peat prepared from a solution pH 4.5 exposed to 28–30 ppbv of ozone.

reactive than ozone and more selective. Both can accept electrons. Many studies also show that the water content highly affects the HA structure and finally its reactivity [*Balnois et al.*, 1999; *Ge et al.*, 2006; *Guo and Ma*, 2006; *Plaschke et al.*, 1999; *Redwood et al.*, 2005; *Widayati and Tan*, 1997]. Fractal dimension (FD) is used to determine the actual space occupied by a system. FD value slowly increases up to 65–70% relative humidity (RH) indicating an expansion of the HA structure and hydration of the most soluble humic acid moieties [*Redwood et al.*, 2005]. These changes can possibly explain the small increase of the ozone uptake coefficient observed with increasing humidity in the dark.

[35] Under near-UV irradiation the uptake coefficient drops from $(3.3 \pm 0.7) \times 10^{-5}$ at 18% RH to $(1.2 \pm 0.2) \times 10^{-5}$ at 65% RH, with a 66% reduction in reactivity. The humidity dependence on HA coatings observed in the present study is very similar to that observed on solid films of benzophenone by *Jammoul et al.* [2008]. The inverse dependence on water partial pressure was there explained by the competitive adsorption of water molecules at the surface and by their quenching activity toward the excited species [*Jammoul et al.*, 2008; *Stemmler et al.*, 2006, 2007].

4.6. Effect of the Solution pH

[36] Since both HA structure [*Balnois et al.*, 1999; *Myneni et al.*, 1999; *Plaschke et al.*, 1999; *Sutton and Sposito*, 2005] and ozone reactivity [*Staehelin and Hoigné*, 1983, 1985; *von Gunten*, 2003] are highly dependent on the pH in aqueous solutions, the O_3 loss on HA Aldrich thin coatings has been investigated as a function of the acidity, which was varied via the pH of the starting solution used to prepare the coatings (see Figure 6). The ozone loss was evaluated after 40 min of exposure, since the dark experiments showed strong initial ozone uptake, which rapidly decreased to a steady state value. The pH dependence shows qualitative similar trends under different light conditions. For the dark experiments the uptake coefficients ranged from (0.8 ± 0.2) to $(1.9 \pm 0.6) \times 10^{-6}$ and ozone varied from 50 to 150 ppbv; the dark experiment did not show a strong dependence on the ozone concentration. Indeed the two data points at pH 9 correspond to 90 ppbv (upper open circle) and 50 ppbv (lower open circle) of ozone. The experiments under visible irradiation show a similar behavior, although the uptake coefficients were larger, ranging from (1.8 ± 0.4) to $(4.5 \pm 1.1) \times 10^{-6}$ at 40–70 ppbv of ozone. In the near-UV experiments, the uptake coefficients reached an upper value of $(10.5 \pm 1.9) \times 10^{-6}$ at pH 9 at ozone concentrations varied from 45 to 60 ppbv.

[37] In solution, when the pH is gradually increased, deprotonation of the most soluble moieties occurs (first carboxylic, then alcoholic and finally phenolic functionalities), and the electrostatic repulsion generated by the charge increment promotes expansion of the structure [*Alvarez-Puebla et al.*, 2006; *Balnois et al.*, 1999; *Myneni et al.*, 1999; *Plaschke et al.*, 1999]. Ozone uptake on HA coatings and submicron aerosol resulted to be sensitive to the degree of deprotonation (basic conditions), although the experiments were performed in solid substrates. And it is known that during drying, both structure and pH can vary. Despite the differences between an aqueous solution and a coating, the uptake coefficients were remarkably enhanced for starting solutions at pH $\geq$ 8, when deprotonation of phenolic-type functionalities begins. This behavior is consistent with previous studies of phenols and humic acid ozonation in solution [*Augugliaro and Rizzuti*, 1978; *Guittonneau et al.*, 1996; *Hoigne and Bader*, 1983; *Mvula and von Sonntag*, 2003; *Ovechkin et al.*, 1977]. The proposed mechanism at such pHs involves phenolate-type ion formation and its further fast reaction with ozone to give ozonide radical ($O_3^{\bullet -}$) followed by O_2 and $O^{\bullet -}$ formation that in solution leads to OH radical formation [*Staehelin and Hoigné*, 1985]. This argument does not completely explain the pH

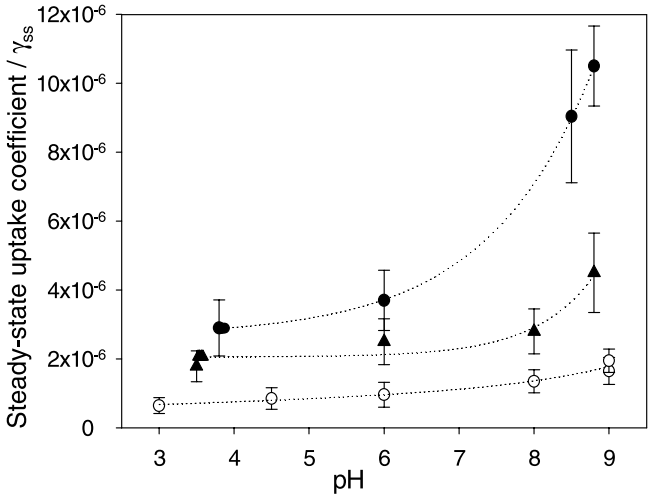

Figure 6. Ozone uptake coefficients on HA Aldrich coating (7 μg cm^{-2}) at different pH under different light conditions (where solid circles, solid triangles, and open circles correspond to UV-A, visible, and dark experiments, respectively). Irradiation is that used at the IRCELYON setup (see Figure 1). The experiments are performed at RH $\leq$ 5% and 293K. The ozone mixing ratio varied from 45 to 60 ppbv in the UV-A experiment, 40–70 ppbv in the visible experiment, and 50–150 ppbv during dark exposure.

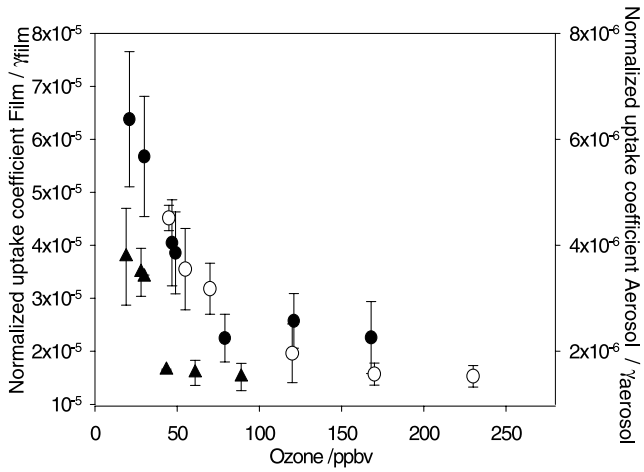

Figure 7. Dependence of the "UV-A flux-normalized" uptake coefficients of O_3 on HA Aldrich. The solid circles correspond to the thin coating experiments at PSI (8 μg cm^{-2}, pH 4.5, 25% RH); the open circles correspond to the experiments at IRCELYON (7 μg cm^{-2}, pH 6, $\leq$5% RH). The solid triangles indicate the submicron particles experiment (solution of 20 g L^{-1}, pH 4.5, 25% RH). The reactive uptakes are normalized with respect to the irradiance reaching the Earth surface in the range 300–420 nm using the photons flux and ozone dependence of the uptake coefficient.

dependence observed in the irradiated experiments. This behavior can be tentatively clarified by the presence of deprotonated species for which, under light exposure, the electron transfer is faster than from protonated phenolic moieties.

4.7. Comparison Aerosol and Films Results

[38] The "near-UV flux-normalized" uptake coefficients of thin coatings (solid and open circles) and submicron airborne particles (solid triangle) of Aldrich HA are presented in Figure 7. The kinetic values were obtained by scaling the measured ones to UV irradiance reaching the Earth surface, using the procedure explained in Figure 3. The coating experiments, performed using two different experimental setups, show a remarkably good quantitative agreement, while the ozone reactivity on HA submicron particles is approximately an order of magnitude smaller. Such discrepancy is mainly explained by the different conditions encountered in the two types of experiments. The main reason arises from the high uncertainty (overestimation) of the surface to volume ratio for the coating experiments. As we do not know the exact film rough structure, using the geometric surface (flat surface) introduces an approximation which can account for a factor of 5–10 uncertainty in the film surface area. For the aerosol experiment, the surface to volume ratio is quite well defined through the SMPS measurement. In addition to this major difference between the two types of experiments a minor explanation for the kinetics discrepancy exists. The aerosol was produced by nebulizing a HA solution at pH 4.5 and such low pH caused the partial precipitation of the heavier moieties (humins and humics), enriching the aerosol with the lighter organic fraction which is mainly constituted by the fulvic fraction. We therefore tested the ozone reactivity on a thin film of fulvic acid under weak near-UV irradiation using the setup 1 (IRCELYON setup 1). Under dry condition (5%RH) with 30 ppbv ozone with an uptake of $(2.4 \pm 0.6) \times 10^{-6}$ was measured, which corresponds approximately to a third of the value of humic acids coating under comparable experimental conditions. When normalized to the Earth surface irradiance this uptake is scaled to $(1.3 \pm 0.4) \times 10^{-5}$. Overestimation of the S/V ratio for the coating and introduction of an aerosol rich in fulvic type fraction and poor in humic and humin fraction, which is much closer to the values observed for the aerosol experiment, can explain this factor 10 of discrepancy between the aerosol and film experiments.

4.8. Gas-Phase Products

[39] In addition to the uptake kinetics we also investigated emissions of VOCs from HA Aldrich coatings upon light and ozone exposure. A clean Pyrex tube was exposed to 73 ppbv ozone to investigate possible VOC artifacts or impurities. Experiment 1 was carried out with 7.2 μg cm^{-2} of HA being exposed to 68 ppbv of ozone, experiment 2 with 10 μg cm^{-2} of HA being exposed to 78 ppbv of ozone. Both coated and uncoated flow tubes were exposed to the trace gas for 20 min in the presence of near-UV radiation (total irradiance 7.7×10^{14} photons cm^{-2} s^{-1} in the range 300–420 nm). The 20-min-time-integrated ozone uptake was 574 ppbv min and 654 ppbv min for experiments 1 and 2, respectively. For the "blank" tube an uptake of 89 ppb min (corresponding to 13–15% of the ozone uptake observed in presence of HA) was observed. Seventy-five percent of the ozone loss on the "blank" Pyrex tube occurred during the first 5 min of exposure. This indicates that in spite of accurate cleaning, some residual contamination was initially present on the glass tube. Table 2 reports all m/z signals (corrected for blank values) for which the observed 20-min-time-integrated increase in mixing ratios exceeded 6 ppbv min (corresponding to $\sim$1% of the observed time-integrated ozone uptake). A compound assignment for the m/z signals is given in Table 2 together with the observed 20-min-time-integrated increase in product mixing ratios for experiments 1 and 2, respectively. For the m/z = 47 signal (formic acid) an increase was observed for sample 1, but not for sample 2. We also observed an increase in m/z = 101 (unidentified), but for this signal the "blank" was not reproducible. The column "Light only" in Table 2 indicates the ion signals that showed an increase even if the samples were exposed to near-UV light only (without ozone). As shown in Table 2, methanol, HCHO, acetaldehyde, acetone, acetic acid or hydroxy-acetaldehyde, hexanal, octanal and nonanal were observed with ozone and light present. Most of the small compounds ($\leq C_3$) were also observed under the "Light only" condition, while emission of longer aldehydes was observable only in the presence of the oxidant. The C_6, C_8 and C_9 aldehydes may originate from ozonolysis of double bonds present in fatty acids [*Hatanaka*, 1993; *Loreto et al.*, 2006]. Small VOCs are commonly emitted from decomposing organic material (as demethylation of pectin from cell walls) [*Fall et al.*, 1999; *Galbally and Kirstine*, 2002; *Loreto et al.*, 2006] or may be induced by photolysis. Our findings suggest that the forma-

Table 2. Compound Assignment for the PTR-MS Signals That Increased When HA Films Were Exposed to O_3 and Light[a]

		Experiment 1		Experiment 2		
m/z	Compound Assignment	Increase, ppbv min	Yield,[b] %	Increase, ppbv min	Yield,[b] %	Light Only
31	formaldehyde	48	8.4	47	7.2	Yes
33	methanol	22	3.8	26	3.9	Yes
43	acetic acid (and/or hydroxy-acetaldehyde): fragment ($-H_2O$)	N/A[c]		N/A[c]		Yes
45	acetaldehyde	29	5.1	45	6.9	Yes
59	acetone (and/or propanal)	23	4.0	28	4.3	Yes
61	acetic acid (and/or hydroxy-acetaldehyde)	N/A[c]		N/A[c]		Yes
69	pentanal, octanal, nonanal: fragment	N/A[d]		N/A[d]		
83	hexanal; fragment ($-H_2O$)	6	1.0	18	2.8	
111	octanal; fragment ($-H_2O$)	19	3.3	23	3.5	
143	nonanal	40	6.9	31	4.7	

[a]Increase denotes the observed 20-min-time-integrated increase in product mixing ratios. Light Only denotes the signals for which an increase was also observed in the presence of light only (no ozone).
[b]Molecular Yield in percent with respect to ozone consumed.
[c]No calibration available.
[d]Fragment of multiple compounds; no quantification.

tion of small VOCs ($\leq C_3$) is not triggered by ozonolysis but more detailed studies are needed to quantify the relative contributions of near-UV light and ozone, respectively, to the observed emissions.

5. Conclusions and Environmental Implications

[40] The present work shows for the first time the photo-enhanced ozone uptake on HA films and submicron aerosols. Under dark conditions, ozone exhibits a small uptake coefficient ($\leq 4 \times 10^{-6}$) onto solid coatings with a weak inverse dependence on the ozone mixing ratio. Under visible irradiation the uptake coefficient increases to 1.0 (± 0.6) $\times 10^{-5}$ for HA Aldrich and to 3.0 (± 0.6) $\times 10^{-5}$ for Pahokee Peat; while under near-UV irradiation the uptake increases up to 7.8 (± 0.9) $\times 10^{-5}$ for Aldrich HA. In both cases the overall kinetics shows a clear inverse dependence on the O_3 partial pressure. The light induced process shows a small time dependence for the first 10–20 min and then stabilizes at a constant level for several hours.

[41] PTR-MS studies on VOC emissions upon irradiation and ozone exposure indicated the formation of small aldehydes (formaldehyde, acetaldehyde, hexanal, octanal, nonanal), methanol and acetone. All the products together account for a total yield of 32–33% of the ozone lost. Additional, albeit not compelling, evidence was found for the formation of formic and acetic acid. Further measurements are needed to establish if our observations are also relevant for the atmospheric budgets of these VOCs at certain sites.

[42] The experimental results on films of humic acids indicated that light-induced depletion of ozone may be directly relevant for exposed soil or soil dust at the Earth surface providing a new mechanism for the diurnal variation of ozone deposition to the ground. Indeed, when the geometric uptake is scaled using the irradiance at the Earth surface the uptake under visible irradiation reaches $\sim 5 \times 10^{-5}$. Using an uptake of $5–10 \times 10^{-5}$, representative of ozone capture under natural irradiation at ground, and taking into account the near-UV and visible contribution, we obtain a photoinduced ozone deposition velocity of 4.5–9 mm s^{-1} using the following formula, $\nu_d = \gamma \cdot \langle c \rangle / 4$ [*Clifford et al.*, 2008]. The total ozone deposition velocity is highly variable depending on various parameters such as vegetation, season, temperature, humidity, and wind conditions. On forest and agricultural areas, average dry deposition during daytime varies from 10 to 60 mm s^{-1} [*Altimir et al.*, 2004; *Cieslik and Gerosa*, 2005; *Cieslik*, 2004; *Ferretti et al.*, 2007; *Fowler et al.*, 2001; *Fuhrer*, 2000; *Massman*, 1993; *Matsuda et al.*, 2005; *Michou et al.*, 2005; *Wesely and Hicks*, 2000; *Zhang et al.*, 2002]. The deposition via stomata of plant leaves is estimated to account for 30–70% of the total dry deposition in the boundary layer [*Altimir et al.*, 2004; *Cieslik and Gerosa*, 2005; *Cieslik*, 2004; *Fuhrer*, 2000]. Therefore an ozone deposition of 4.5–9 mm s^{-1} obtained by for light induced ozone destruction onto humic substances represents a nonnegligible fraction of the total dry deposition and should accordingly be taken into account when modeling ozone deposition on natural and agricultural soil.

[43] Even though the reactivity of ozone with humic substances observed here remains hypothetical with respect to its representativeness for the reactivity of organic aerosol, few statements about organic aerosol processing can be made. While the process is certainly not able to affect the gas-phase ozone budget anywhere in the troposphere, the amount of ozone reacted may be significant for aerosol aging. The likely product of an electron transfer process to O_3 is OH, which is very reactive. If we consider a particle with 100 nm diameter, an ozone mixing ratio of 40 ppbv and an uptake coefficient of 4×10^{-6}, the amount of O_3 molecules taken up per second into one particle with a surface area of 1.3×10^{-9} cm^2 is 9.3 per second or 4×10^5 in 12 h. If the potential product OH is formed at the surface, roughly 1×10^{15} molecules per cm^2 surface have become available (equivalent to about one monolayer). If we assume a bulk process, i.e., dividing the 4×10^5 by the volume, 5.2×10^{-16} cm^3, roughly 1.3 mol/L are taken up and OH has been generated (and likely reacted) during the course of 12 h. Both these numbers indicate that even a

relatively small uptake coefficient for O_3 could lead to significant processing of the condensed phase of the particles.

[44] **Acknowledgments.** This work has been partly supported by EUCAARI (European Integrated project on Aerosol Cloud Climate and Air Quality interactions) 036833-2 and by European Science Foundation through the INTROP scientific program and by the EU FP6 ACCENT Access to Infrastructures initiative. Birger Bohn contributed to the irradiance measurements of the PSI aerosol flow reactor and coated wall flow tube.

References

Altimir, N., J.-.P. Tuovinen, T. Vesala, M. Kulmala, and P. Hari (2004), Measurements of ozone removal by Scots pine shoots: Calibration of a stomatal uptake model including the non-stomatal component, *Atmos. Environ.*, *38*(15), 2387–2398, doi:10.1016/j.atmosenv.2003.09.077.

Alvarez-Puebla, R., C. Valenzuela-Calahorro, and J. J. Garrido (2006), Theoretical study on fulvic acid structure, conformation and aggregation—A molecular modelling approach, *Sci. Total Environ.*, *358*(1–3), 243–254.

Ammann, M., E. Roessler, R. Strekowski, and C. George (2005), Nitrogen dioxide multiphase chemistry: Uptake kinetics on aqueous solutions containing phenolic compounds, *Phys. Chem. Chem. Phys.*, *7*, 2513–2518.

Amy, G. L., C. J. Kuo, and R. A. Sierka (1988), Ozonation of humic substances: Effects on molecular weight distributions of organic carbon and trihalomethane formation potential, *Ozone Sci. Eng.*, *10*(1), 39–54.

Arens, F., L. Gutzwiller, H. W. Gaggeler, and M. Ammann (2002), The reaction of NO_2 with solid anthrarobin (1,2,10-trihydroxy- anthracene), *Phys. Chem. Chem. Phys.*, *4*, 3684–3690.

Augugliaro, V., and L. Rizzuti (1978), The pH dependence of the ozone absorption kinetics in aqueous phenol solutions, *Chem. Eng. Sci.*, *33*, 1441–1447.

Balnois, E., K. J. Wilkinson, J. R. Lead, and J. Buffle (1999), Atomic force microscopy of humic substances: Effects of pH and ionic strength, *Environ. Sci. Technol.*, *33*(21), 3911–3917.

Baltensperger, U., et al. (2005), Secondary organic aerosols from anthropogenic and biogenic precursors, *Faraday Discuss.*, *130*, 265–278.

Barrie, L. A., J. W. Bottenheim, R. C. Schnell, P. J. Crutzen, and R. A. Rasmussen (1988), Ozone destruction and photochemical-reactions at polar sunrise in the lower arctic atmosphere, *Nature*, *334*, 138–141.

Batjes, N. H. (1996), Total carbon and nitrogen in the soils of the world, *Eur. J. Soil Sci.*, *47*, 151–163.

Cappiello, A., E. De Simoni, C. Fiorucci, F. Mangani, P. Palma, H. Trufelli, S. Decesari, M. C. Facchini, and S. Fuzzi (2003), Molecular characterization of the water-soluble organic compounds in fogwater by ESIMS/MS, *Environ. Sci. Technol.*, *37*(7), 1229–1240.

Chiang, Y.-P., Y.-Y. Liang, C.-N. Chang, and A. C. Chao (2006), Differentiating ozone direct and indirect reactions on decomposition of humic substances, *Chemosphere*, *65*(11), 2395–2400.

Cho, M., H. Kim, S. H. Cho, and J. Yoon (2003), Investigation of ozone reaction in river waters causing instantaneous ozone demand, *Ozone Sci. Eng.*, *25*(4), 251–259.

Cieslik, S. A. (2004), Ozone uptake by various surface types: a comparison between dose and exposure, *Atmos. Environ.*, *38*(15), 2409–2420.

Cieslik, S., and G. Gerosa (2005), Ozone flux data used to assess damage risk to vegetation, *Phyton*, *45*(4), 261–266.

Clifford, D., D. J. Donaldson, M. Brigante, B. D'anna, and C. George (2008), Reactive uptake of ozone by chlorophyll at aqueous surfaces, *Environ. Sci. Technol.*, *42*(4), 1138–1143.

Cooney, D. O., S. S. Kim, and E. J. Davis (1974), Analyses of mass-transfer in hemodialyzers for laminar blood-flow and homogeneous dialysate, *Chem. Eng. Sci.*, *29*, 1731–1738.

Decesari, S., M. C. Facchini, E. Matta, M. Mircea, S. Fuzzi, A. R. Chughtai, and D. M. Smith (2002), Water soluble organic compounds formed by oxidation of soot, *Atmos. Environ.*, *36*(11), 1827–1832.

Decesari, S., et al. (2006), Characterization of the organic composition of aerosols from Rondonia, Brazil, during the LBA-SMOCC 2002 experiment and its representation through model compounds, *Atmos. Chem. Phys.*, *6*(2), 375–402.

de Gouw, J., and C. Warneke (2007), Measurements of volatile organic compounds in the Earth's atmosphere using proton-transfer-reaction mass spectrometry, *Mass Spectrom. Rev.*, *26*(2), 223–257.

Dinar, E., T. F. Mentel, and Y. Rudich (2007), The density of humic acids and humic like substances (HULIS) from fresh and aged wood burning and pollution aerosol particles, *Atmos. Chem. Phys.*, *6*(12), 5213–5224.

Dinar, E., A. Abo Riziq, C. Spindler, C. Erlick, G. Kiss, and Y. Rudich (2008), The complex refractive index of atmospheric and model humic-like substances (HULIS) retrieved by a cavity ring down aerosol spectrometer (CRD-AS), *Faraday Discuss.*, *137*, 279–295.

Dommen, J., A. Metzger, J. Duplissy, M. Kalberer, M. R. Alfarra, A. Gascho, E. Weingartner, A. S. H. Prevot, B. Verheggen, and U. Baltensperger (2006), Laboratory observation of oligomers in the aerosol from isoprene/NO_x photooxidation, *Geophys. Res. Lett.*, *33*, L13805, doi:10.1029/2006GL026523.

Emeline, A. V., V. K. Ryabchuk, and N. Serpone (2005), Dogmas and misconceptions in heterogeneous photocatalysis: Some enlightened reflections, *J. Phys. Chem. B*, *109*(39), 18,515–18,521.

Fall, R., T. Karl, A. Hansel, A. Jordan, and W. Lindinger (1999), Volatile organic compounds emitted after leaf wounding: On-line analysis by proton transfer-reaction mass spectrometry, *J. Geophys. Res.*, *104*, 15,963–15,974.

Ferretti, M., et al. (2007), Measuring, modelling and testing ozone exposure, flux and effects on vegetation in southern European conditions—What does not work? A review from Italy, *Environ. Pollut.*, *146*(3), 648–658.

Fowler, D., C. Flechard, J. N. Cape, R. L. Storeton-West, and M. Coyle (2001), Measurements of ozone deposition to vegetation quantifying the flux, the stomatal and non-stomatal components, *Water Air Soil Pollut.*, *130*(1–4), 63–74.

Fuhrer, J. (2000), Introduction to the special issue on ozone risk analysis for vegetation in Europe, *Environ. Pollut.*, *109*(3), 359–360.

Fuller, E. N., K. Ensley, and J. C. Giddings (1969), Diffusion of halogenated hydrocarbons in helium: The effect of structure on collision cross sections, *J. Phys. Chem.*, *73*(11), 3679–3685.

Galbally, I. E., and W. Kirstine (2002), The production of methanol by flowering plants and the global cycle of methanol, *J. Atmos. Chem.*, *43*, 195–229.

Garcia-Araya, J. F., J. P. Croue, R. J. Beltran, and B. Legube (1995), Origin and conditions of ketoacid formation during ozonation of natural organic matter in water, *Ozone Sci. Eng.*, *17*(6), 647–656.

Ge, X. P., Y. M. Zhou, C. H. Lu, and H. X. Tang (2006), AFM study on the adsorption and aggregation behavior of dissolved humic substances on mica, *Sci. China, Ser. B*, *49*(3), 256–266.

George, C., R. S. Strekowski, J. Kleffmann, K. Stemmler, and M. Ammann (2005), Photoenhanced uptake of gaseous NO_2 on solid organic compounds: A photochemical source of HONO?, *Faraday Discuss.*, *130*, 195–210.

Gonzalez-Perez, J. A., F. J. Gonzalez-Vila, G. Almendros, and H. Knicker (2004), The effect of fire on soil organic matter—A review, *Environ. Int.*, *30*(6), 855–870.

Gorski, Z., P. Grobelny, and J. Slawinski (1996), The effect of UV-radiation and ozone on humus substances, *Curr. Top. Biophys.*, *20*(2), 128–133.

Graber, E. R., and Y. Rudich (2006), Atmospheric HULIS: How humic-like are they? A comprehensive and critical review, *Atmos. Chem. Phys.*, *6*, 729–753.

Gueymard, C. A., D. Myers, and K. Emery (2002), Proposed reference irradiance spectra for solar energy systems testing, *Sol. Energy*, *73*, 443–467. (Available at http://rredc.nrel.gov/solar/spectra/am1.5/#Gueymard2)

Guittonneau, S., D. Thibaudeau, and P. Meallier (1996), Free radicals formation induced by the ozonation of humic substances in aqueous medium, *Catal. Today*, *29*(1–4), 323–327.

Guo, J., and J. Ma (2006), AFM study on the sorbed NOM and its fractions isolated from River Songhua, *Water Res.*, *40*, 1975–1984.

Hatanaka, A. (1993), The biogeneration of green odour by green leaves, *Phytochemistry*, *34*, 1201–1218.

Hauglustaine, D. A., G. P. Brasseur, S. Walters, P. J. Rasch, J. F. Muller, L. K. Emmons, and M. A. Carroll (1998), MOZART, a global chemical transport model for ozone and related chemical tracers: 2. Model results and evaluation, *J. Geophys. Res.*, *103*, 28,291–28,335.

Hausmann, M., and U. Platt (1994), Spectroscopic measurement of bromine oxide and ozone in the high Arctic during Polar Sunrise Experiment 1992, *J. Geophys. Res.*, *99*, 25,399–25,413.

Hoffer, A., G. Kiss, M. Blazsó, and A. Gelencsér (2004), Chemical characterization of humic-like substances (HULIS) formed from a lignin-type precursor in model cloud water, *Geophys. Res. Lett.*, *31*, L06115, doi:10.1029/2003GL018962.

Hofzumahaus, A., A. Kraus, and M. Müller (1999), Solar actinic flux spectroradiometry: A technique for measuring photolysis frequencies in the atmosphere, *Appl. Opt.*, *38*(21), 4443–4460.

Hoigne, J., and H. Bader (1983), Rate constants of reactions of ozone with organic and inorganic-compounds in water: 1. Non-dissociating organic-compounds, *Water Res.*, *17*, 173–183.

Holmes, B. J., and G. A. Petrucci (2006), Water-soluble oligomer formation from acid-catalyzed reactions of levoglucosan in proxies of atmospheric aqueous aerosols, *Environ. Sci. Technol.*, *40*(16), 4983–4989.

Jacob, D. J. (2000), Heterogeneous chemistry and tropospheric ozone, *Atmos. Environ.*, *34*(12–14), 2131–2159.

Jammoul, A., S. Gligorovski, C. George, and B. D'anna (2008), Photosensitized heterogeneous chemistry of ozone on organic films, *J. Phys. Chem. A*, *112*(6), 1268–1276.
Janzen, H. H. (2004), Carbon cycling in Earth systems—A soil science perspective, *Agric. Ecosyst. Environ.*, *104*, 399–417.
Kirchstetter, T. W., T. Novakov, and P. V. Hobbs (2004), Evidence that the spectral dependence of light absorption by aerosols is affected by organic carbon, *J. Geophys. Res.*, *109*, D21208, doi:10.1029/2004JD004999.
Kruithof, J. C., M. A. van der Goag, and D. van der Kooy (1989), Effect of ozonation and chlorination on humic substances in water, *ACS Symp. Ser.*, *219*, 663–680.
Lindinger, W., A. Hansel, and A. Jordan (1998), Proton-transfer-reaction mass spectrometry (PTR-MS): Online monitoring of volatile organic compounds at pptv levels, *Chem. Soc. Rev.*, *27*(5), 347–354.
Loreto, F., C. Barta, F. Brilli, and I. Nogues (2006), On the induction of volatile organic compound emissions by plants as consequence wounding or fluctuations of light and temperature, *Plant Cell Environ.*, *29*(9), 1820–1828.
Mallevialle, J., Y. Laval, M. Lefebvre, and C. Rousseau (1978), The degradation of humic substances in water by various oxidation agents (ozone, chlorine, chlorine dioxide), in *Ozone/Chlorine Dioxide Oxidation Products of Organic Materials*, pp. 189–199, Ozone Press Int., Detroit, Mich.
Massman, W. J. (1993), Partitioning ozone fluxes to sparse grass and soil and the inferred resistances to dry deposition, *Atmos. Environ., Part A*, *27A*(2), 167–174.
Matsuda, K., I. Watanabe, V. Wingpud, P. Theramongkol, P. Khummongkol, S. Wangwongwatana, and T. Totsuka (2005), Ozone dry deposition above a tropical forest in the dry season in northern Thailand, *Atmos. Environ.*, *39*(14), 2571–2577.
Mayol-Bracero, O. L., P. Guyon, B. Graham, G. Roberts, M. O. Andreae, S. Decesari, M. C. Facchini, S. Fuzzi, and P. Artaxo (2002), Water-soluble organic compounds in biomass burning aerosols over Amazonia: 2. Apportionment of the chemical composition and importance of the polyacidic fraction, *J. Geophys. Res.*, *107*(D20), 8091, doi:10.1029/2001JD000522.
McNeill, V. F., G. M. Wolfe, and J. A. Thornton (2007), The oxidation of oleate in submicron aqueous salt aerosols: Evidence of a surface process, *J. Phys. Chem. A*, *111*(6), 1073–1083.
Michou, M., P. Laville, D. Serca, A. Fotiadi, P. Bouchou, and V. H. Peuch (2005), Measured and modeled dry deposition velocities over the ESCOMPTE area, *Atmos. Res.*, *74*(1–4), 89–116.
Mmereki, B. T., and D. J. Donaldson (2003), Direct observation of the kinetics of an atmospherically important reaction at the air-aqueous interface, *J. Phys. Chem. A*, *107*(50), 11,038–11,042.
Mmereki, B. T., D. J. Donaldson, J. B. Gilman, T. L. Eliason, and V. Vaida (2004), Kinetics and products of the reaction of gas-phase ozone with anthracene adsorbed at the air-aqueous interface, *Atmos. Environ.*, *38*(36), 6091–6103.
Mochida, M., Y. Katrib, J. T. Jayne, D. R. Worsnop, and S. T. Martin (2007), The relative importance of competing pathways for the formation of high-molecular-weight peroxides in the ozonolysis of organic aerosol particles, *Atmos. Chem. Phys.*, *6*(12), 4851–4866.
Mvula, E., and C. von Sonntag (2003), Ozonolysis of phenols in aqueous solution, *Org. Biomol. Chem.*, *1*(10), 1749–1756.
Myneni, S., J. T. Brown, G. A. Martinez, and W. Meyer-Ilse (1999), Imaging of humic substance macromolecular structures in water and soils, *Science*, *286*(5443), 1335–1337.
Nawrocki, J., and I. Kalkowska (1999), Humic and fulvic acids as precursors of aldehydes-ozonation by-products, *Toxicol. Environ. Chem.*, *68*(3–4), 297–306.
Ovechkin, V. S., M. L. Konstantinova, and S. D. Razumovskii (1977), Effect of the pH of the medium on the kinetics and the mechanism of ozone reaction with phenol, in *Vsesoyuznaya Mezhvuzovskaya Konferentsiya po Ozonu*, 2nd ed., edited by Y. A. Mal'tsev, pp. 124–125, Moscow Univ., Moscow.
Plaschke, M., J. Romer, R. Klenze, and J. I. Kim (1999), In situ AFM study of sorbed humic acid colloids at different pH, *Colloids Surf. A*, *160*(3), 269–279.
Poeschl, U., T. Letzel, C. Schauer, and R. Niessner (2001), Interaction of ozone and water vapor with spark discharge soot aerosol particles coated with benzo[a]pyrene: O_3 and H_2O adsorption, benzo[a]pyrene degradation, and atmospheric implications, *J. Phys. Chem. A*, *105*(16), 4029–4041.
Rapoport, V. L., B. M. Antipenko, and M. G. Malkin (1968), Photosorption of hydrogen and methane on titanium dioxide, *Kinet. Katal.*, *9*(6), 1306–1314.
Redwood, P. S., J. R. Lead, R. M. Harrison, I. P. Jones, and S. Stoll (2005), Characterization of humic substances by environmental scanning electron microscopy, *Environ. Sci. Technol.*, *39*(7), 1962–1966.
Reinhardt, A., C. Emmenegger, B. Gerrits, C. Panse, J. Dommen, U. Baltensperger, R. Zenobi, and M. Kalberer (2007), Ultrahigh mass resolution and accurate mass measurements as a tool to characterize oligomers in secondary organic aerosols, *Anal. Chem.*, *79*(11), 4074–4082.
Salma, I., and G. G. Lang (2008), How many carboxyl groups does an average molecule of humic-like substances contain?, *Atmos. Chem. Phys.*, *8*, 5997–6002.
Staehelin, J., and J. Hoigne (1983), Reaction mechanism and kinetics of ozone decomposition in water in the presence of organic substances, *Vom Wasser*, *61*, 337–348.
Staehelin, J., and J. Hoigne (1985), Decomposition of ozone in water in the presence of organic solutes acting as promoters and inhibitors of radical chain reactions, *Environ. Sci. Technol.*, *19*(12), 1206–1213.
Stemmler, K., M. Ammann, C. Donders, J. Kleffmann, and C. George (2006), Photosensitized reduction of nitrogen dioxide on humic acid as a source of nitrous acid, *Nature*, *440*, 195–198.
Stemmler, K., M. Ndour, Y. Elshorbany, J. Kleffmann, B. D'anna, C. George, B. Bohn, and M. Ammann (2007), Light induced conversion of nitrogen dioxide into nitrous acid on submicron humic acid aerosol, *Atmos. Chem. Phys.*, *7*, 4237–4248.
Sutton, R., and G. Sposito (2005), Molecular structure in soil humic substances: The new view, *Environ. Sci. Technol.*, *39*(23), 9009–9015.
Swietlik, J., A. Dabrowska, U. Raczyk-Stanislawiak, and J. Nawrocki (2004), Reactivity of natural organic matter fractions with chlorine dioxide and ozone, *Water Res.*, *38*, 547–558.
Swift, R. S. (2001), Sequestration of carbon by soil, *Soil Sci.*, *166*, 858–871.
Thomson, J., A. Parkinson, F. A. Roddick, B. Legube, and M. Müller (2004), Depolymerization of chromophoric natural organic matter, *Environ. Sci. Technol.*, *38*(12), 3360–3369.
von Gunten, U. (2003), Ozonation of drinking water: Part I. Oxidation kinetics and product formation, *Water Res.*, *37*, 1443–1467.
Wesely, M. L., and B. B. Hicks (2000), A review of the current status of knowledge on dry deposition, *Atmos. Environ.*, *34*(12–14), 2261–2282.
Widayati, S., and K. H. Tan (1997), Atomic force microscopy of humic acid, *Commun. Soil Sci. Plant Anal.*, *28*(3–5), 189–196.
York, D. (1966), Least-squares fitting of a straight line, *Can. J. Phys.*, *44*(5), 1079–1086.
Yu, M. J., Y. H. Kim, I. Han, and H. C. Kim (2002), Ozonation of Han River humic substances, *Water Sci. Technol.*, *46*(11–12), 21–26.
Zhang, L., J. R. Brook, and R. Vet (2002), On ozone dry deposition—With emphasis on non-stomatal uptake and wet canopies, *Atmos. Environ.*, *36*(30), 4787–4799.

M. Ammann, S. Fahrni, and K. Stemmler, Laboratory of Radio and Environmental Chemistry, Paul Scherrer Institute, CH-5232 Villigen, Switzerland.
B. D'Anna, C. George, and A. Jammoul, UMR5256, Institut de Recherches sur la Catalyse et l'Environnement de Lyon, Université Lyon 1, CNRS, F-69626 Villeurbanne, France. (barbara.danna@ircelyon.univ-lyon1.fr)
A. Wisthaler, Institut für Ionenphysik und Angewandte Physik, Universität Innsbruck, Technikerstrasse 25, A-6020 Innsbruck, Austria.